ADVANCED FUNCTIONAL MATERIALS

Supporting Information

for *Adv. Funct. Mater.*, DOI: 10.1002/adfm.202000948

Fermi Level Engineering of Passivation and Electron Transport Materials for p-Type $CuBi_2O_4$ Employing a High-Throughput Methodology

Zemin Zhang, Sarah A. Lindley, Dan Guevarra, Kevin Kan, Aniketa Shinde, John M. Gregoire, Weihua Han, Erqing Xie, Joel A. Haber, and Jason K. Cooper**

Fermi Level Engineering of Passivation and Electron Transport Materials for p-type $CuBi_2O_4$ Employing A High Throughput Methodology

Zemin Zhang,[1,3,†] *Sarah A. Lindley,*[1,†] *Dan Guevarra,*[4] *Kevin Kan,*[4] *Aniketa Shinde,*[4] *John M. Gregoire,*[4] *Weihua Han,*[3] *Erqin Xie,*[3] *Joel A. Haber,*[4,*] *Jason K. Cooper,*[1,2,*]

[1]Joint Center for Artificial Photosynthesis, [2]Chemical Sciences Division, Lawrence Berkeley National Laboratory, Berkeley, California 94720, United States.

[3]School of Physical Science and Technology, Lanzhou University, Lanzhou, 730000, China

[4]Joint Center for Artificial Photosynthesis, California Institute of Technology, Pasadena CA 91125, USA.

†These authors contributed equally.

*Corresponding Author: jkcooper@lbl.gov, jahaber@caltech.edu

Keywords: p-type semiconductor, passivation layer, high-throughput methology, fermi level engineering, solar photochemistry

Supporting Figures：

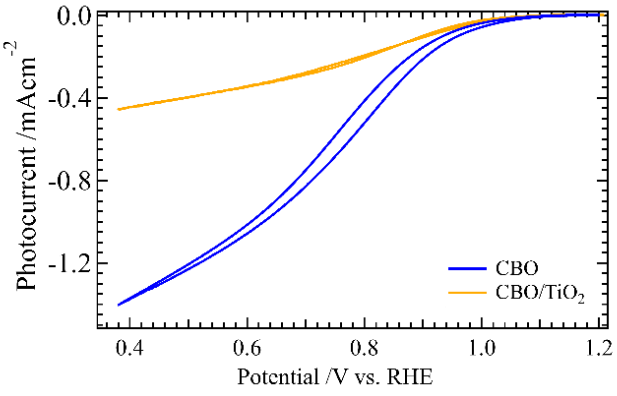

Figure S1. The J-V response of CBO photocathode before (blue) and after (orange) 2 nm TiO_2 overlayer deposition by ALD.

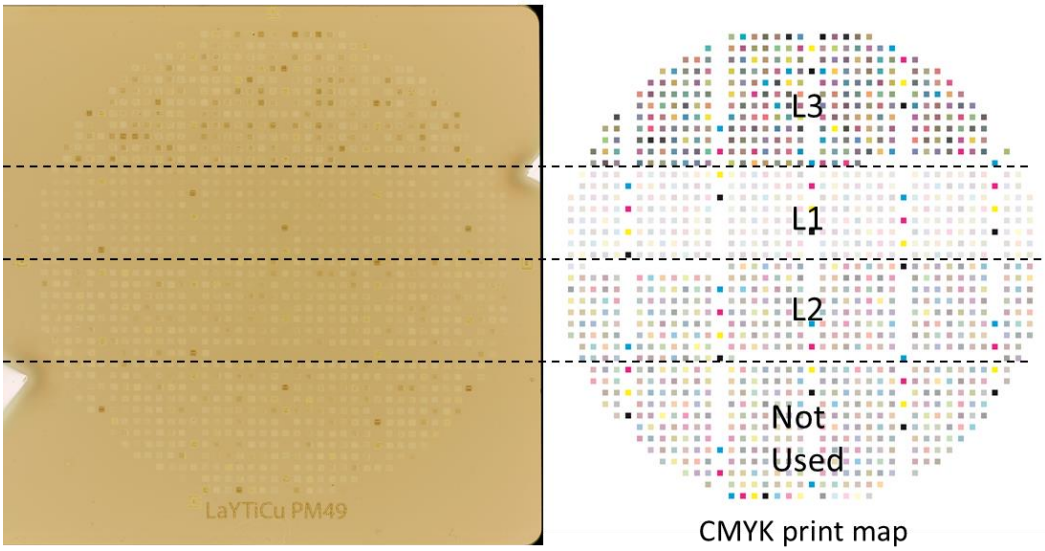

Figure S2. Photo image of the La:Y:Ti:Cu oxide coating library on CBO/FTO film with the corresponding print map indicating the different loading regions.

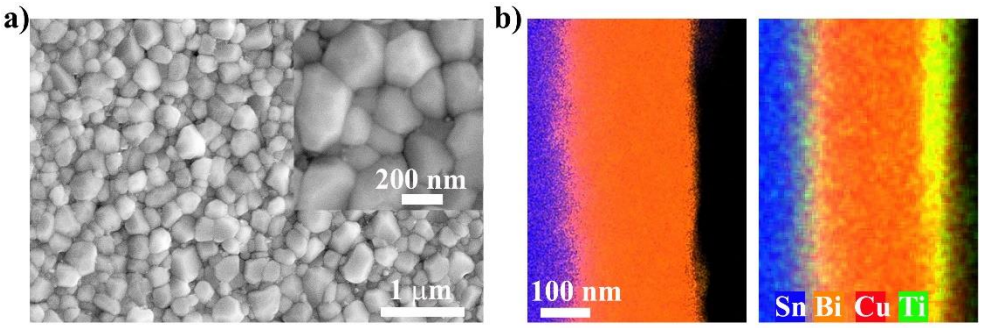

Figure S3. SEM image of CBO sample with $Cu_xTi_yO_z$ overlayer (a); high resolution cross-section EDX mapping of CBO and CBO/$Cu_xTi_yO_z$ samples (b).

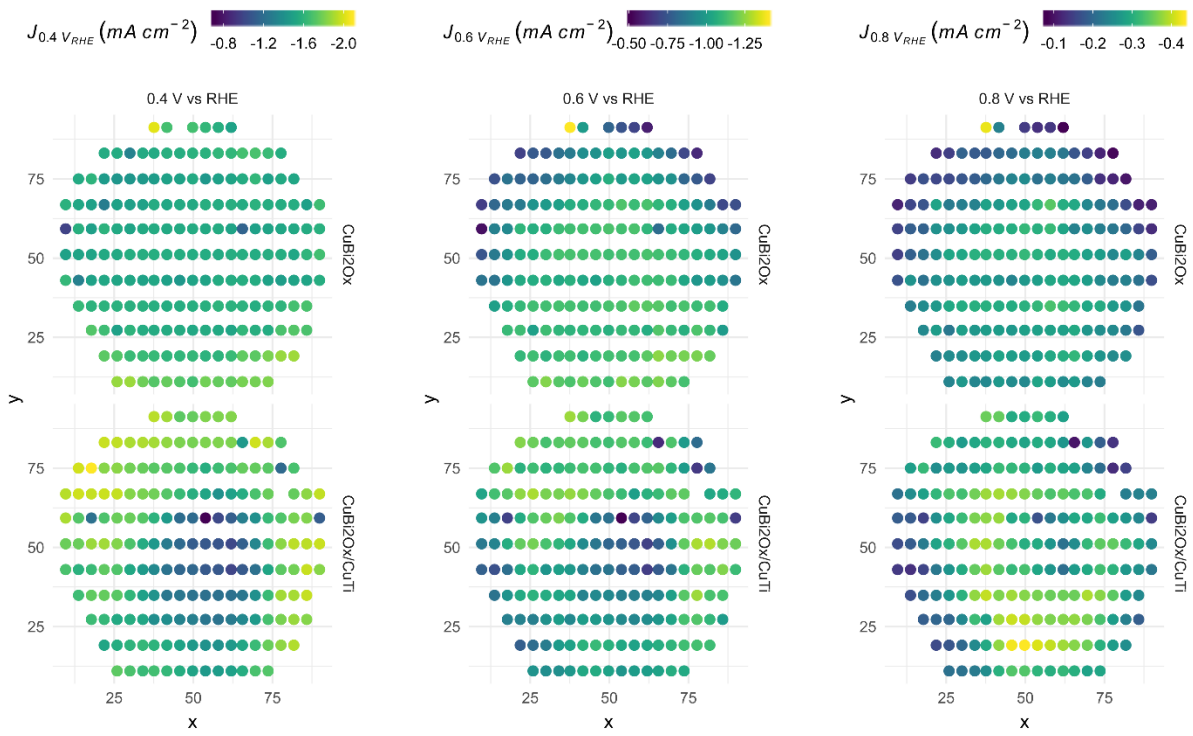

Figure S4. The photocurrent maps of CBO (top, a, c, e) and CBO/$Cu_xTi_yO_z$ (bottom, b, d, f) photocathodes under different applied potential.

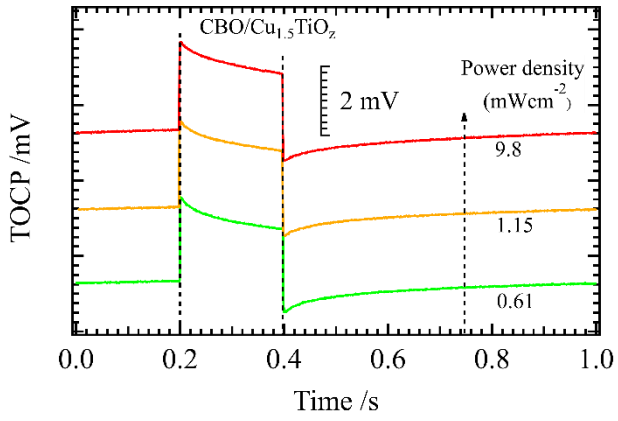

Figure S5. Transient open-circuit potential measurements of CBO/$Cu_{1.5}TiO_z$ film under continuous white light bias and pulsed blue light with variable density in 0.1 M $KHCO_3$

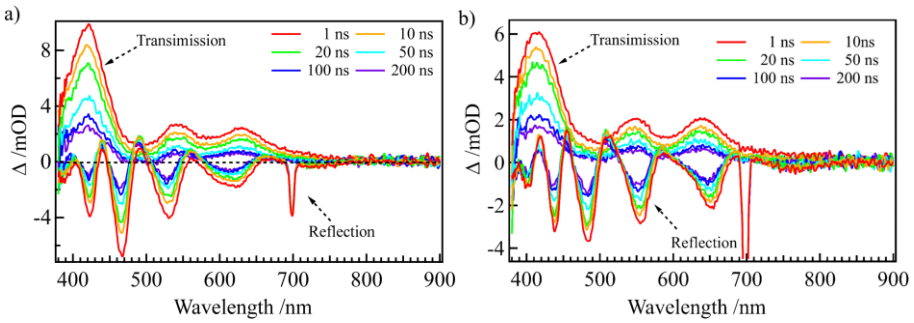

Figure S6. Differential transmission (dT) and differential reflection spectra (dR) of CBO (a) and CBO/$Cu_{1.5}TiO_z$ (b) film films at various pump-probe delays.

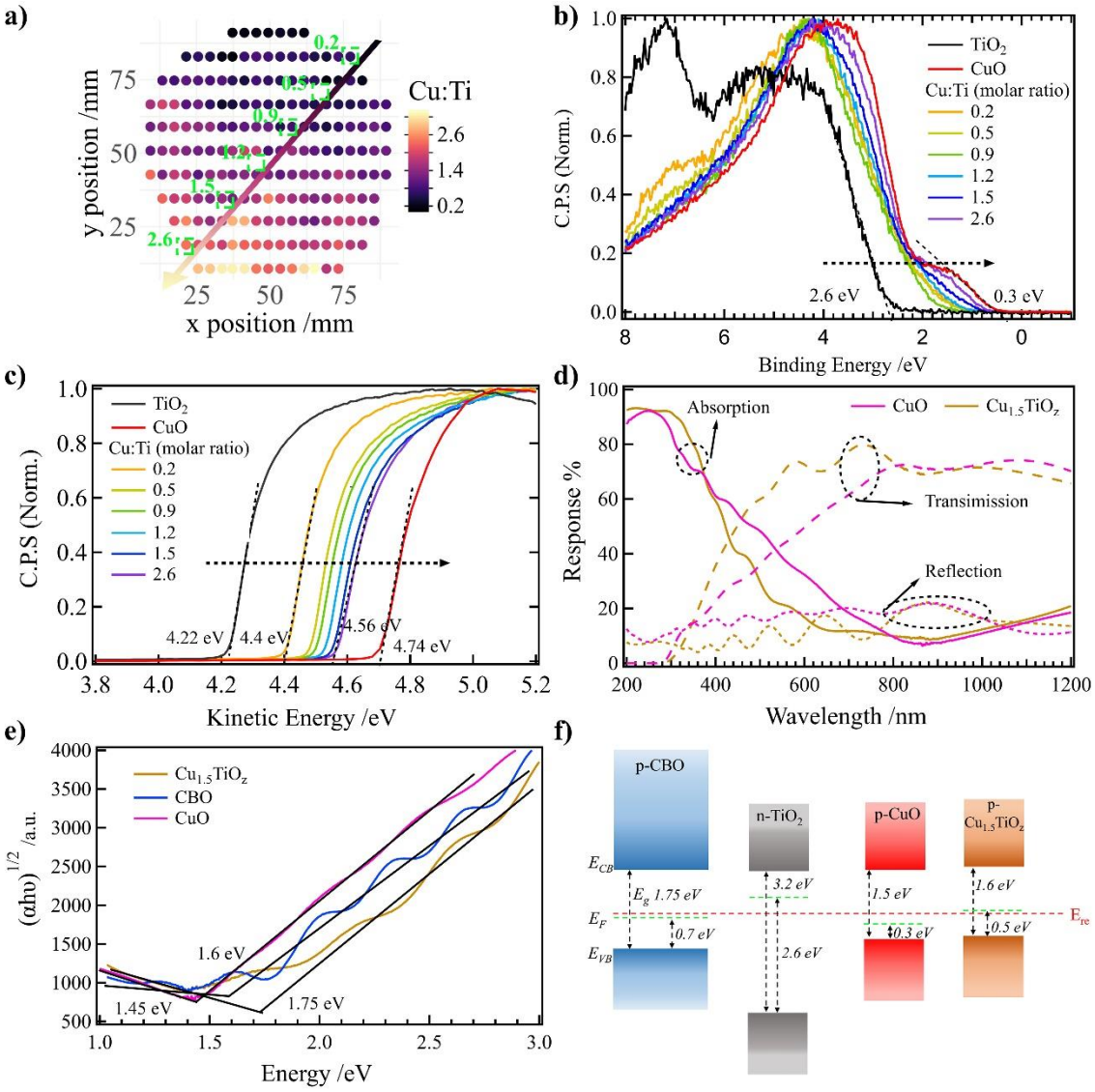

Figure S7. The composition map of $Cu_xTi_yO_z$ overlayer showing the six selected points with Cu:Ti ratio of 0.2, 0.5, 0.9, 1.2, 1.5, and 2.6(a); the Valence band edge (b) and second electron cut-off spectra

of the six selected points, CBO, TiO_2, and CuO (c); Transmission, reflection and absorption spectroscopy of CuO and $Cu_{1.5}TiO_z$ films (d); Tauc plots of CuO, CBO, and $Cu_{1.5}TiO_z$ films (e); Band alignment of CBO, TiO_2, CuO, and $Cu_{1.5}TiO_z$ films (f) in electrolyte containing 0.1 M KHCO3 and 0.1 M Na2S2O8 (pH=8.2) with reduction potential (E_{re}) at 0.12 V_{RHE} (-4.56 V_{vacuum}).

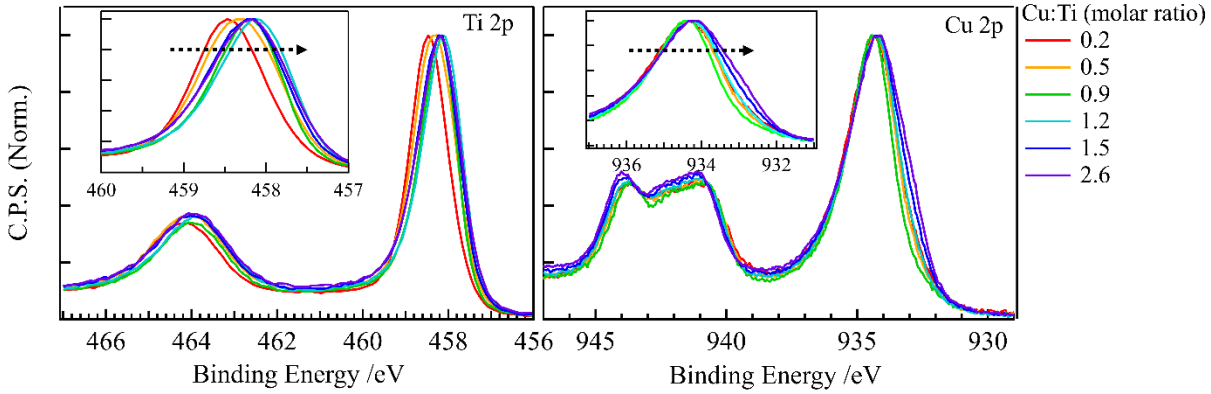

Figure S8. The core-level XPS spectra of Ti 2p and Cu 2p for $Cu_xTi_yO_z$ overlayer with six selected Cu:Ti ratios.

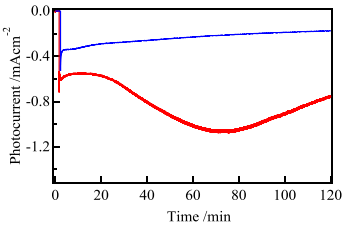

Figure S9. The J-t curves of CBO (blue) and CBO/$Cu_{1.5}TiO_z$ (red) photocathode at 0.8 V_{RHE} under blue LED illumination over the course of 120 min.

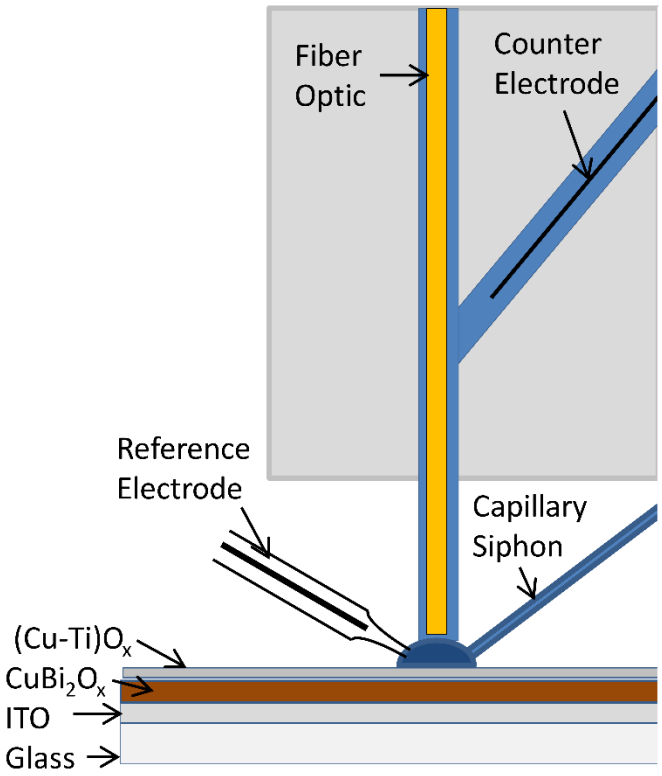

Figure S10. Cross-sectional diagram of the scanning droplet cell.